

## Disturbance of Tunneling Coherence by Oxygen Vacancy in Epitaxial Fe/MgO/Fe Magnetic Tunnel Junctions

G. X. Miao,<sup>1,\*</sup> Y. J. Park,<sup>1,2</sup> and J. S. Moodera<sup>1</sup>

<sup>1</sup>*Francis Bitter Magnet Laboratory, Massachusetts Institute of Technology, Cambridge, Massachusetts 02139, USA*

<sup>2</sup>*Center for Spintronics Research, Korea Institute of Science and Technology, Seoul, 136-791, South Korea*

M. Seibt,<sup>3</sup> G. Eilers,<sup>3</sup> and M. Münzenberg<sup>3</sup>

<sup>3</sup>*IV. Physikalisches Institut, Universität Göttingen, Göttingen, Germany*

(Received 4 April 2008; published 19 June 2008)

Oxygen vacancies in the MgO barriers of epitaxial Fe/MgO/Fe magnetic tunnel junctions are observed to introduce symmetry-breaking scatterings and hence open up channels for noncoherent tunneling processes that follow the normal WKB approximation. The evanescent waves inside the MgO barrier thus experience two-step tunneling, the coherent followed by the noncoherent process, and lead to lower tunnel magnetoresistance, *higher* junction resistance, as well as increased bias and temperature dependence. The characteristic length of the symmetry scattering process is determined to be about 1.6 nm.

DOI: [10.1103/PhysRevLett.100.246803](https://doi.org/10.1103/PhysRevLett.100.246803)

PACS numbers: 73.40.Gk, 72.10.Fk, 72.25.-b, 85.75.-d

Ten years after the successful demonstration of room temperature (RT) tunnel magnetoresistance (TMR) with Al<sub>2</sub>O<sub>3</sub> tunnel barriers [1], giant TMR in epitaxial [2] and textured [3] MgO based magnetic tunnel junctions (MTJs) are reported, with the TMR at RT reaching 410% in molecular beam epitaxy (MBE) grown samples [4], and over 500% in sputtered samples [5]. The giant TMR is a direct consequence of coherent tunneling process [6,7], in which both the electrons' spins and their Bloch states symmetry are conserved, in contrast to the traditional tunneling process that only conserves spins [8]. Epitaxial Fe/MgO/Fe MTJ structure is shown to yield TMR value up to 180% at RT, and an effective tunnel barrier height of 0.39 eV [2]. The lower than expected resistance in MgO based MTJs have been a puzzling issue for a long time. Such low apparent tunnel barrier height is consistent with the theoretical calculations [6] but still a surprising observation because the band gap of MgO is as high as 7.5 eV in post annealed 2.7 nm MgO [9]. The discrepancy is partially because within MgO the effective mass of electrons with  $\Delta_1$  symmetry is only 0.37 times that of free electrons [10], and using the correct effective mass will yield a barrier height of about 1 eV, still much lower than what one expects from the *I-V* curve fittings [11]. This brings up another source for the discrepancy: the Bloch states form evanescent waves within the MgO barrier and the corresponding decay rates are determined by the complex energy bands of the same symmetry in the barrier [6]. As one can easily see from Fig. 8 in Ref. [6], the decay rates of the Bloch states within the MgO energy gap do not follow the expected Wentzel-Kramers-Brillouin (WKB) approximation, which should have projection of a straight line on that plot. Especially, it is clear that states with  $\Delta_1$  symmetry have a much slower decay rate than that expected from the WKB approximation, resulting in the widely observed low barrier height in MgO based MTJs. Attempting to fit the *I-V* curve in these MgO based MTJs leads to unphysical

numbers indicating the failure of the WKB model in this system [11]. Thus, the apparent low barrier height is also a sign of the deviation from WKB approximation in these symmetry filtering barriers [12] and is unique to the coherent tunneling process. Any disturbance on the Bloch wave coherence is expected to result in profound effects.

In this Letter we aim to look at the effect of inherent growth related defects on the overall tunneling process, leading to a better understanding of coherent tunneling phenomena and opening up new ways of tuning the tunnel barrier properties. Oxygen vacancies are known to cause charge neutral gap states in MgO at about 1.2 eV below the conduction band minimum [13], and this has an effect of dramatically lowering tunnel barrier height. As suggested in [9], elastic scatterings from oxygen vacancies can open up parallel cotunneling channels that short-circuit the coherent tunneling process. Here, we experimentally demonstrate that by varying the oxygen vacancy we can effectively tune the properties of the MgO tunnel barrier, and clearly demonstrate the superposition of two parallel conduction channels, the symmetry-coherent tunneling process that has an effective barrier height of 0.39 eV and the normal spin-coherent tunneling process that has a nominal barrier height of 0.82 eV. The tunneling properties in the low voltage bias and low temperature region are shown to be dominated by the former process, while in the high bias and high temperature region mainly by the latter process. The possibility of tuning the MgO barrier properties by controlling the growth condition is very important for practical purposes, especially for those utilizing double barrier structures, such as in the hot field of spin transfer torque based devices [14], and the hot electron spin injection devices [15].

We fabricate our MTJ structure on Si(100) substrate in an ultrahigh vacuum system, with the base pressure better than  $1 \times 10^{-10}$  torr. The Si substrate is cleaned sequentially in acetone, isopropyl alcohol, diluted sulfuric acid

(9%), isopropyl alcohol, and diluted HF (10%), in order to obtain hydrogen terminated surface before loading into the MBE chamber. Because of the large lattice mismatch between MgO and Si ( $\sim 3.4\%$ ), the establishment of epitaxy of MgO on Si is nontrivial, whereas it is of technological importance for the potential spin injection purpose. MgO is  $e$ -beam evaporated from single crystal sources, and we found that a thickness of 10 nm MgO was necessary to obtain good epitaxy, and also a deposition temperature of  $300^\circ\text{C}$  was required. The buffer layer further serves as a diffusion barrier between Si and Fe. After the deposition of the buffer layer, the bottom Fe electrode of 20 nm is deposited at  $180^\circ\text{C}$  at a rate of  $0.6\text{ nm/min}$ , which yields a flat self-constructed surface [16]. X-ray  $\theta$ - $2\theta$  diffraction and pole figure confirmed the epitaxy of the MgO layer and the Fe layer on top of it, but a large broadening of the diffraction peaks (rocking curve FWHM  $\sim 7^\circ$  for MgO and  $\sim 3^\circ$  for Fe) indicates that the layers have some dispersion in their epitaxial growth orientations. The MgO tunnel barrier was deposited at different temperatures with a very slow rate of  $0.25\text{ nm/min}$ . Residual gas analyzer showed the main gas remaining in the MBE chamber during the MgO deposition is oxygen. The MgO barrier formed by  $e$ -beam evaporating MgO source in MBE is known to be oxygen deficient [2,9]. Having the same gas removal efficiency (two cryopumps plus the chamber shroud cooled at  $77\text{ K}$ ), the substrate temperature can effectively change the stoichiometry of the MgO film. Specifically, higher deposition temperature can result in stronger affinity of MgO to oxygen, making it more stoichiometric. After the formation of the MgO barrier, the top Fe electrode was deposited at  $200^\circ\text{C}$ . In order to separate the coercivity of the bottom and top Fe layers, we deposited  $5\text{ nm Fe}$  as the top electrode and magnetically hardened with an additional  $20\text{ nm Co}$  on top. The whole structure was then annealed *in situ* at  $310^\circ\text{C}$  for  $1.5\text{ h}$ , and a  $5\text{ nm Au}$  capping layer was deposited at RT as the last step. The MTJs were patterned with standard optical lithography with junction areas of  $4 \times 6\ \mu\text{m}^2$ .

We focus our attention on two types of MTJs, both with  $2.5\text{ nm MgO}$  barrier and deposited at  $180^\circ\text{C}$  and RT, respectively. In order to make direct comparison, the samples shown here are deposited in the same run, identical in every step except for the deposition of MgO barrier, such that the only variable here is the barrier deposition temperature, and the resultant oxygen vacancies. Other minor structural differences have been taken care of by the high temperature annealing step in the end. The time between the deposition of the  $180^\circ\text{C}$  and that of the RT barrier is less than  $20\text{ min}$  under a background pressure of  $1 \times 10^{-10}\text{ torr}$ , and no noticeable changes have been reported for Fe surfaces under such conditions [17]. Figure 1 shows the TMR loops for these MTJs at RT and  $1\text{ K}$ . In the samples with barrier deposited at  $180^\circ\text{C}$ , we achieved over  $130\%$  TMR at RT and over  $190\%$  at  $1\text{ K}$ . These samples are taken as reference samples for the discussion: their TMR

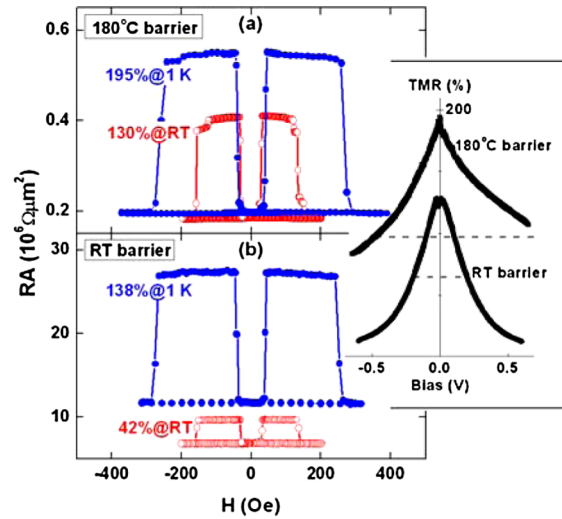


FIG. 1 (color online). Comparison of the magnetoresistance (MR) loops at RT and  $1\text{ K}$  for MTJs of the same  $2.5\text{ nm MgO}$  barrier thickness but deposited at  $180^\circ\text{C}$  (a) and RT (b). Inset shows the corresponding TMR bias dependence at  $1\text{ K}$ .

dependence on temperature and bias are quite consistent with the coherent tunneling phenomena [2,3,6,7]. The resistance/conductance of spin parallel (P) configuration is only marginally dependent on temperature [Fig. 1(a)] and bias [Fig. 2(c)], and the corresponding  $I$ - $V$  curve is nearly linear [Fig. 2(a)]. In comparison, the resistance/conductance of spin antiparallel (AP) configuration shows noticeably larger temperature [Fig. 1(a)] and bias dependence [Fig. 2(c)], and the  $I$ - $V$  curve is significantly non-linear [Fig. 2(a)]. Consequently, the temperature and bias dependence of TMR are mainly from the AP contributions, whereas the electron transport in P configuration is largely free-electron-like [12].  $V_{\text{half}}$  (where TMR reaches half its zero bias value) in these junctions is over  $0.6\text{ V}$  at RT,

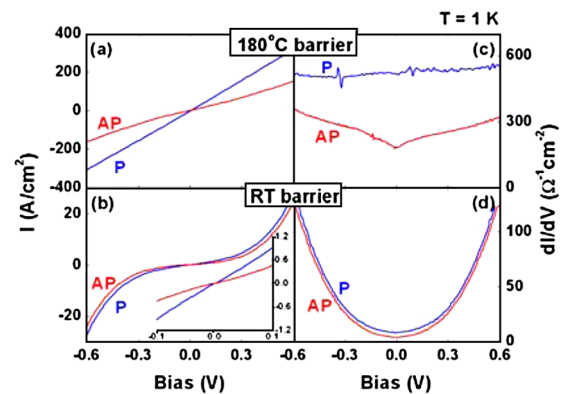


FIG. 2 (color online). Comparison of the  $I$ - $V$  and  $dI/dV$  curves of the MTJs with  $2.5\text{ nm MgO}$  barrier deposited at  $180^\circ\text{C}$  (a),(c) and RT (b),(d), the curves of spin-P (blue) and spin-AP (red) configurations are marked. Inset shows the low bias ( $<100\text{ mV}$ ) region of the MTJ with RT deposited barrier. Measurement is performed at  $1\text{ K}$ .

further confirming the high quality of these junctions. Though our maximum TMR is lower than the 180% RT record [2], it is worth pointing out that the samples are deposited on Si wafers and thus of broader interest, especially for the purpose of spin injection into Si that takes hot electron approaches [15]. The lower TMR can be attributed to the fairly large lattice mismatch between the MgO buffer layer and the Si substrate ( $\sim 3.4\%$ ), which introduces quite a few lattice distortions.

The behavior of MTJs with RT deposited MgO barriers is quite different from the previously described standard samples. First, the TMR is much lower at RT, being only 42%, and rises very fast to 138% with the lowering of temperature [Fig. 1(b)]. A large temperature dependence of the junction resistance in both P and AP configurations is observed [Fig. 1(b)]. Second, a dramatic reduction of  $V_{\text{half}}$  is observed in the TMR bias dependence (Fig. 1 inset), and the  $I$ - $V$  curves become significantly nonlinear as well [Fig. 2(b)]. Third, the conductance rises fast with increasing bias voltage [Fig. 2(d)], roughly following a parabolic behavior, indicating the presence of an elastic tunneling conduction channel with fairly low tunnel barrier height [8]. The above features consistently suggest that in addition to the expected symmetry-conserving conduction, there exist additional conduction channels mediated by oxygen vacancies and allow spins to tunnel through, even though they do not possess the best matched Bloch symmetry. Certain activation energy is apparently required, and at low bias and low temperature the large TMR is mostly preserved ( $>130\%$ ) owing to the coherent tunneling process, yet at higher temperature and higher bias TMR suffers greatly. The  $I$ - $V$  curve in low bias region (Fig. 2 inset) closely resembles the  $I$ - $V$  curve of the reference sample [Fig. 2(a)], whereas at high bias it deviates dramatically.

A rough estimate of the defect energy level can be obtained by fitting of the  $I$ - $V$  data in Fig. 2(b) to Brinkman's model [18]. Using the P state conductance curve in the  $\pm 0.3$  V range, the fitting yields the effective tunnel barrier height  $\sim 0.83$  eV, barrier thickness  $\sim 2.7$  nm, and a negligible barrier asymmetry  $\sim 0.03$  eV. The estimated barrier height is reasonable considering that the oxygen vacancies are located 1.2 eV below the conduction band minimum [13], and the new Fermi level is somewhere above the vacancy states. We can also estimate the strength of the symmetry scattering using our obtained TMR values. We assume the two tunneling processes through the MgO barrier are the coherent tunneling and the noncoherent tunneling. Here coherent and noncoherent are referring to the Bloch symmetry, and we neglect all spin flipping such that the spin is assumed to be conserved. As illustrated in Fig. 3, we start by simplifying the incident electron wave as consisting of only one symmetry state, and this state loses its symmetry in the barrier due to scatterings. The scattered waves then enter the noncoherent tunneling process in a two step process. In the spin  $P$  state

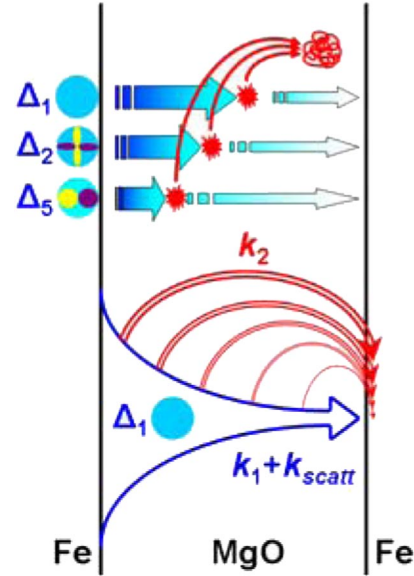


FIG. 3 (color online). Schematic illustration of the noncoherent tunneling process. The lateral angular momentum of an incoming electron is conserved until a scattering happens, and the electron loses its coherence and enters the noncoherent tunneling process, which has a much larger decay wave vector inside the barrier.

the conduction is dominated by the  $\Delta_1$  symmetry, and the two contributions can be separated: first, a decay wave vector for the coherent tunneling process is determined by the decay rate of the  $\Delta_1$  symmetry; second, a decay wave vector for the noncoherent subsequent tunneling process given by an effective barrier height  $\varphi_{\text{ox}}$  determined by the oxygen defect band, respectively,

$$k_1 \cong 6.4 \text{ nm}^{-1} \quad k_2 = \frac{2}{\hbar} \sqrt{2m\varphi_{\text{ox}}}$$

Here  $k_1$  and  $k_2$  are the decay wave vector in the coherent and noncoherent processes,  $m$  is the free-electron mass (it is a valid assumption for noncoherent tunneling process, similar to the cases in amorphous  $\text{Al}_2\text{O}_3$  barriers), and  $\varphi_{\text{ox}}$  is the tunnel barrier height in the noncoherent process. For  $k_1$  the value for  $\Delta_1$  symmetry is taken [2]. To account for the loss of coherence in tunneling, we introduce a symmetry scattering vector  $k_{\text{scatt}}$ , and the probability for the initial incident wave to cross the barrier without losing its symmetry is reduced to

$$T_1 = \exp[-(k_1 + k_{\text{scatt}})d],$$

and the probability of the scattered wave to cross the barrier via a noncoherent two-step process is given by summing over all possible processes for a scattering event at depth  $x$  in the barrier,

$$T_2 = \int_0^d k_{\text{scatt}} \exp[-(k_1 + k_{\text{scatt}})x] \times \exp\left[-\frac{2(d-x)}{\hbar} \sqrt{2m\varphi_{\text{ox}}}\right] dx.$$

Here  $k_{\text{scatt}} \exp[-(k_1 + k_{\text{scatt}})x]dx$  registers the portion of the coherent wave that goes to noncoherent process in the interval  $dx$ . The resultant TMR will be the summation of contributions from both channels,

$$\frac{T_1 + T_2}{1 + \text{TMR}} = \frac{T_1}{1 + \text{TMR}_1} + \frac{T_2}{1 + \text{TMR}_2}.$$

Here TMR,  $\text{TMR}_1$ , and  $\text{TMR}_2$  denote the TMR for the overall process, the coherent process, and the noncoherent process, respectively, and  $T_i/(1 + \text{TMR}_i)$  [ $i = 1, 2$ ] gives the transmission in the AP configuration. We take our reference sample (with 180 °C deposited barrier) TMR results as  $\text{TMR}_1$ , whereas  $\text{TMR}_2$  can be estimated to be 38% from Julliere's model [19] by assuming 40% spin polarization in Fe [8]. Applying the above derived model to our oxygen-deficient sample (with RT deposited barrier), we find that the symmetry scattering wave vector  $k_{\text{scatt}}$  is 0.614 nm<sup>-1</sup> at 1 K and zero bias. This corresponds to a characteristic scattering length for the symmetry-breaking oxygen vacancy centers of 1.6 nm, or about 7 monolayers.

An interesting prediction from the above simple model is that the junction resistance will be largely increased with the presence of noncoherent tunneling processes. This is a consequence of the removal of the more conductive coherent currents, and the generation of less conductive noncoherent currents. Note the introduction of  $k_{\text{scatt}}$  does not lead to any resistance change by itself, because if one sets  $k_2 = k_1$ ,  $k_{\text{scatt}}$  cancels and the initial transmission coefficient is restored. The decay wave vectors of the two types of currents are  $k_1 = 6.4 \text{ nm}^{-1}$  [2,6] and  $k_2 = 9.3 \text{ nm}^{-1}$  as determined from our analysis. Using these numbers, we can further estimate a 5-times increase of the resistance area (RA) product in the P state due to the presence of noncoherent tunneling. Experimentally, we observed an increase of about 40 times. We need to be cautious in interpreting the larger RA increase, because other factors are also taking part in the junction resistance change. First, the film deposited at lower temperature has better homogeneity on the bottom electrodes, thus making its effective barrier thickness higher than its counterpart deposited at higher temperature. TEM images indeed show increased long range waviness for the higher temperature deposited barriers. Second, some of the scattered waves may enter the other  $\Delta_2$ ,  $\Delta_2'$ , and  $\Delta_5$  symmetry states instead, all of which have larger decay rates compared to  $k_2$ . Our simple model did not consider these tunneling channels because the path opened up by oxygen vacancies should have the lowest decay rate among these channels, though the other paths would inevitably contribute to the increase of the overall resistance. We believe our observed resistance increase is due to the combined effect of the above-mentioned contributions. We note that the dramatic de-

crease of junction resistance as well as increase of TMR with improving barrier stoichiometry is also observed in sputtered samples [20], confirming that our simple model is valid, and not specific to MBE depositions only. On the other hand, sputtered MgO barriers may be complicated from the existence of negatively charged Mg vacancies as well [9,21], making them harder to be interpreted quantitatively.

In conclusion, we demonstrated experimentally the coexistence of coherent and noncoherent tunneling processes for the evanescent waves inside epitaxial the MgO barrier. The latter process is a consequence of the introduction of oxygen vacancies, which lowers the barrier height and opens channels for the noncoherent process. The presence of a small amount of defects is shown to *increase* junction resistance instead. The symmetry scattering characteristic length after which the coherence is lost is estimated to be about 1.6 nm. The results are particularly useful for applications that require tunable barrier properties.

This work is supported by NSF, ONR, and KIST-MIT program.

---

\*gxiao@mit.edu

- [1] J. S. Moodera, L. R. Kinder, T. M. Wong, and R. Meservey, *Phys. Rev. Lett.* **74**, 3273 (1995).
- [2] S. Yuasa *et al.*, *Nat. Mater.* **3**, 868 (2004).
- [3] S. S. P. Parkin *et al.*, *Nat. Mater.* **3**, 862 (2004).
- [4] S. Yuasa *et al.*, *Appl. Phys. Lett.* **89**, 042505 (2006).
- [5] Y. M. Lee *et al.*, *Appl. Phys. Lett.* **90**, 212507 (2007).
- [6] W. H. Butler, X.-G. Zhang, T. C. Schulthess, and J. M. MacLaren, *Phys. Rev. B* **63**, 054416 (2001).
- [7] J. Mathon and A. Umerski, *Phys. Rev. B* **63**, 220403(R) (2001).
- [8] J. S. Moodera and G. Mathon, *J. Magn. Magn. Mater.* **200**, 248 (1999).
- [9] P. G. Mather, J. C. Read, and R. A. Buhrman, *Phys. Rev. B* **73**, 205412 (2006).
- [10] W. H. Butler *et al.*, *IEEE Trans. Magn.* **41**, 2645 (2005).
- [11] C. W. Miller *et al.*, *Phys. Rev. B* **74**, 212404 (2006).
- [12] G. X. Miao *et al.*, *J. Appl. Phys.* **99**, 08T305 (2006).
- [13] A. Gibson, R. Haydock, and J. P. LaFemina, *Phys. Rev. B* **50**, 2582 (1994).
- [14] Z. T. Diao *et al.*, *Appl. Phys. Lett.* **90**, 132508 (2007).
- [15] I. Appelbaum, B. Q. Huang, and D. J. Monsma, *Nature (London)* **447**, 295 (2007).
- [16] M. Muller, F. Matthes, and C. M. Schneider, *Europhys. Lett.* **80**, 17007 (2007).
- [17] R. Bertacco *et al.*, *J. Vac. Sci. Technol. A* **16**, 2277 (1998).
- [18] W. F. Brinkman, R. C. Dynes, and J. M. Rowell, *J. Appl. Phys.* **41**, 1915 (1970).
- [19] M. Jullière, *Phys. Lett. A* **54**, 225 (1975).
- [20] Y. S. Choi *et al.*, *Appl. Phys. Lett.* **90**, 012505 (2007).
- [21] J. J. Cha, J. C. Read, R. A. Buhrman, and D. A. Muller, *Appl. Phys. Lett.* **91**, 062516 (2007).